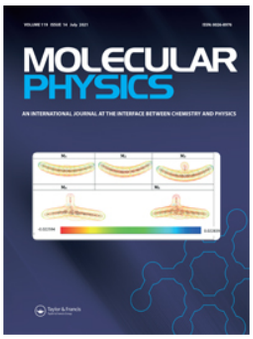

Taylor & Francis
Taylor & Francis Group

Molecular Physics

An International Journal at the Interface Between Chemistry and Physics

ISSN: (Print) (Online) Journal homepage: https://www.tandfonline.com/loi/tmph20

# An *ab initio* study on the bonding in $H_2CO_3$ and related species

Apostolos Kalemos

**To cite this article:** Apostolos Kalemos (2021) An *ab initio* study on the bonding in $H_2CO_3$ and related species, Molecular Physics, 119:14, e1952327, DOI: 10.1080/00268976.2021.1952327

**To link to this article:** https://doi.org/10.1080/00268976.2021.1952327

MOLECULAR PHYSICS
2021, VOL. 119, NO. 14, e1952327 (8 pages)
https://doi.org/10.1080/00268976.2021.1952327

Taylor & Francis
Taylor & Francis Group

RESEARCH ARTICLE

# An *ab initio* study on the bonding in $H_2CO_3$ and related species

Apostolos Kalemos

Department of Chemistry, Laboratory of Physical Chemistry, National and Kapodistrian University of Athens, Athens, Greece

**ABSTRACT**

In the current work we propose an elucidation of the electronic structure of carbonic acid, $H_2CO_3 = (HO)_2CO$, through multi reference configuration interaction methods. We study the formation of both carbonic acid and related species like the parental $H_2CO$ species and the isoelectronic $F_2CO$ molecule along the $X_2C + O$ and $2X + CO$ $C_{2v}$ paths (X = H, F, and OH). The participation of the excited states of their fragments appears to be transparent in the evolution of both the energy profiles and the non adiabatic coupling matrix elements of the corresponding states.

**ARTICLE HISTORY**
Received 18 May 2021
Accepted 1 July 2021

**KEYWORDS**
$H_2CO$; $F_2CO$; $H_2CO_3$; non adiabatic

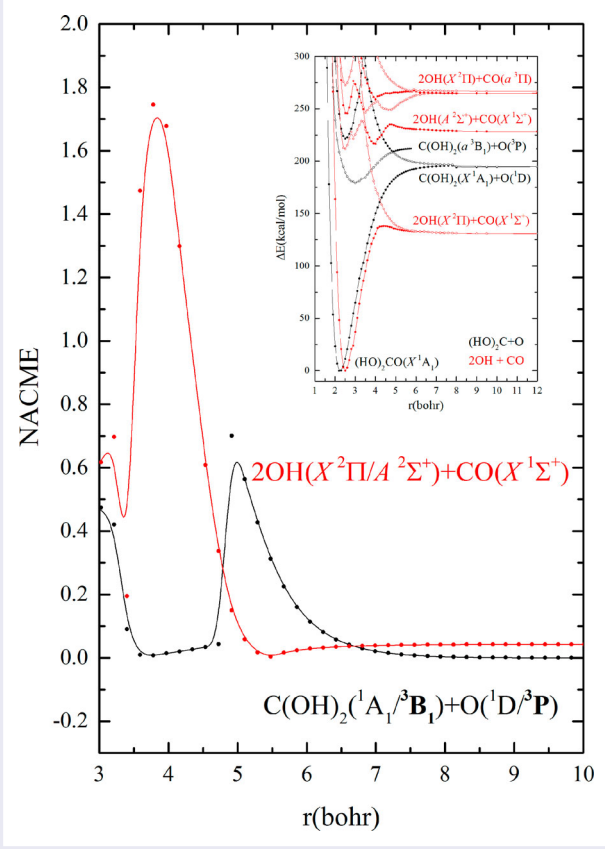


## 1. Introduction

Carbon is one of the most abundant elements in the Universe and on Earth's crust while its' amazing versatility, due to its four valence electrons and the energetic topography of its low lying excited states, contributes to its unique diversity in forming (organic) compounds of simple (*e.g.* $C_2$, $CO_2$, $CH_4$) or complicated (*e.g.* DNA) character and to its unusual and incredible polymer

**CONTACT** Apostolos Kalemos kalemos@chem.uoa.gr Department of Chemistry, Laboratory of Physical Chemistry, National and Kapodistrian University of Athens, Panepistimiopolis, Athens, 157 71 Hellas, Greece

formation ability (*e.g.* graphite, graphene, diamond) that makes it the major building stone of all known life on this planet.

Carbonic acid, $H_2CO_3$, is a representative example of a carbon compound gathering together three of the most abundant elements of the Universe, *i.e.* H, O, and C. It is a diprotic acid with a major role in human biology, in earth's geology, and in extraterrestrial and industrial processes. It plays an incredible role in the evacuation of $CO_2$ in the human body [1], stabilises the pH value of blood and other biological fluids [2], it regulates the global temperature through the solubility of $CO_2$ in the oceans [3], it plays a fundamental role in plant physiology through the $CO_2$ uptake and release of $O_2$ [4], it is responsible for the shelf life of many soft drinks, and it is used in commercial and industrial cooling systems.

Despite its profound importance in so many areas it is an elusive molecular entity since it decomposes rapidly in $CO_2$ and $H_2O$. The very first observation of this species is believed to be a mass spectroscopic detection by Terlouw *et al.* [5], followed by a microwave spectra of its cis − trans monomer [6] and its most stable cis–cis form [7] both by Mori and coworkers and by an infrared detection of its gaseous form trapped in Ne and Ar matrices [8–10]; see also Ref. [11] for an historical account of its experimental detection. Despite the scarcity of experimental work there is a wealthy amount of computational and theoretical work treating several aspects such as energetics, stability, acidity, dehydration, tunnelling splitting and so on; see *e.g.* Refs. [12–24]. But, we are not aware of any computational work studying the way the atoms bind together in order to form this molecule. It is well known that carbon is a tetrahedral atom and this means that all of its four valence electrons *are* or *can* be used in a molecular formation. The archetype of tetrahedral coordination is methane, $CH_4$, a molecule of fundamental importance in chemistry; see *e.g.* Refs. [25] and [26]. Its halide analogue, tetrafluoro methane, $CF_4$, is a very stable gas. Fluorine is isoelectronic to the OH radical but 'curiously' enough $C(OH)_4$ (orthocarbonic acid) does not exist [27]; see also Ref. [28], but its ethylated form ($C(OCH_3)_4$, tetroethoxymethane) does exist and it is even reported as early as 1864 [29]. Considering now the Si analogues we have $SiH_4$ (*vs* $CH_4$), $SiF_4$ (*vs* $CF_4$), and $Si(OH)_4$ (*vs* $C(OH)_4$). The latter species, orthosilicic acid, exists (see *e.g.* Ref. [30]) and has even biological and potential therapeutic effects [31].

In this report we propose to elucidate the electronic structure of carbonic acid ($H_2CO_3 = (HO)_2CO$) along with its isoelectronic species $F_2CO$. Needless to say that the parental molecule is formaldehyde ($H_2CO$) and as such it will be our guide in the following discussions.

## 2. Computational details

Valence single − and multi − reference correlation methods, CCSD(T) and MRCI, respectively, have been used in conjunction with the cc − pVQZ [32] basis set in order to study $H_2CO$, $F_2CO$, and $(HO)_2CO$ ($= H_2CO_3$) along several $C_{2v}$ dissociation/formation paths. Fragmentation species, $CH_2$, $CF_2$, $C(OH)_2$, and CO are also detailed for the sake of completeness. The active space of the zero order CASSCF wavefunctions is of plain valence character, thus comprising all molecular orbitals that arise from the symmetry combination of the 2*s*, 2*p* (C, O, and F) and 1*s* (H) atomic orbitals of the constituent atoms. Single and double valence excitations out of all CASSCF configuration state functions (CSF) were used in the MRCI wavefunctions but for the dissociation/formation of $X_2CO$ (X = F and OH) species along the $X_2C + O$ and $2X + CO$ paths of $C_{2v}$ nature, in which cases a selection threshold of *circa* 0.010/0.015 was applied to the norm of all CSFs for each orbital configuration. In order to monitor the character of the wavefunctions and their evolution along the reaction paths envisaged we have computed the associated non adiabatic coupling matrix elements (NACME) by finite differences at the CASSCF level with a step of 0.01 Å. MOLPRO has been employed for all of our computations [33].

## 3. Results and discussion

As already stated $H_2CO$ is the archetype for the species to be detailed in the present work. It is interesting and revealing at the same time to delve into its electronic structure. One formation path is through the interaction of the isoelectronic species $CH_2$ and O. The ground state of methylene is of $\tilde{X}^3B_1$ symmetry while its first excited state is of $\tilde{a}^1A_1$ symmetry ($T_e$ (exp) $= 8.998 \pm 0.014$ kcal/mol, [34]); see also Refs. [35] and [36] and Table 1 for computational results currently obtained and oxygen's ground and first excited states are of $^3P$ and $^1D$ symmetry ($\Delta E$ (exp) $= 45.1$ kcal/mol, [37]), respectively. Another formation path is through the interaction of CO and two H atoms. Carbon monoxide's ground state, a triply bonded system (see *e.g.* Ref. [38]), is of $X^1\Sigma^+$ symmetry with its first excited state of $a^3\Pi$ symmetry and an excitation energy of $T_e$ (exp) $= 139.2$ kcal/mol [39]. Both dissociation/formation routes, *i.e.* $H_2C + O$ and $2H + CO$, are thought provoking to consider. Formaldehyde's ground state is of singlet spin ($\tilde{X}^1A_1$) symmetry and as such it correlates adiabatically to $CH_2$ ($\tilde{X}^3B_1$) + O ($^3P$) and/or CO ($X^1\Sigma^+$) + 2H ($^2S$). The pictorial representation of their asymptotic fragments on the basis of valence bond Lewis – vbL diagrams is given in Schemes 1 and 2.

**Table 1.** Energies E (hartree) and molecular parameters (bond distances in Å and bond angles in degrees) of the species studied presently.

| Species | −E | Molecular parameters | | | |
|---|---|---|---|---|---|
| CO ($X^1\Sigma^+$) | 113.172 170[a] | 1.132[a] | | | |
| CO ($a^3\Pi$) | 112.947 790[a] | 1.209[a] | | | |
| $CH_2$ ($\tilde{X}^3B_1$) | 39.083 476[a] | 1.077[a]$_{CH}$ | 133.47[a]$_{\angle HCH}$ | | |
| $CH_2$ ($\tilde{a}^1A_1$) | 39.068 216[a] | 1.109[a]$_{CH}$ | 102.05[a]$_{\angle HCH}$ | | |
| $CF_2$ ($\tilde{X}^1A_1$) | 237.430 372[a] | 1.297[a]$_{CF}$ | 104.98[a]$_{\angle FCF}$ | | |
| $CF_2$ ($\tilde{a}^3B_1$) | 237.341 759[a] | 1.313[a]$_{CF}$ | 119.28[a]$_{\angle FCF}$ | | |
| $C(OH)_2$ ($\tilde{X}^1A_1$) | 189.495 940[b] | 1.325[b]$_{CO}$ | 0.960[b]$_{OH}$ | 104.77[b]$_{\angle OCO}$ | 105.87[b]$_{\angle HOC}$ |
| $C(OH)_2$ ($\tilde{a}^3B_1$) | 189.387 534[b] | 1.359[b]$_{CO}$ | 0.960[b]$_{OH}$ | 116.04[b]$_{\angle OCO}$ | 108.00[b]$_{\angle HOC}$ |
| $H_2CO$ ($\tilde{X}^1A_1$) | 114.342 434[a] | 1.206[a]$_{CO}$ | 1.103[a]$_{CH}$ | 116.20[a]$_{\angle HCH}$ | 121.90[a]$_{\angle HCO}$ |
| $H_2CO$ ($\tilde{X}^1A_1$) | 114.369 009[b] | 1.207[b]$_{CO}$ | 1.102[b]$_{CH}$ | 116.45[b]$_{\angle HCH}$ | 121.77[b]$_{\angle HCO}$ |
| $F_2CO$ ($\tilde{X}^1A_1$) | 312.568 924[a] | 1.174[a]$_{CO}$ | 1.312[a]$_{CH}$ | 107.82[a]$_{\angle FCF}$ | 126.09[a]$_{\angle FCO}$ |
| $F_2CO$ ($\tilde{X}^1A_1$) | 312.740 158[b] | 1.173[b]$_{CO}$ | 1.311[b]$_{CH}$ | 107.84[b]$_{\angle FCF}$ | 126.08[b]$_{\angle FCO}$ |
| $(HO)_2CO$ ($\tilde{X}^1A_1$) | 264.740 425[b] | 1.203[b]$_{CO}$ | 1.336[b]$_{C-OH}$ | 108.63[b]$_{\angle (HO)C(OH)}$ | |

[a]MRCI/cc − pVQZ; [b]RCCSD(T)/cc − pVQZ.

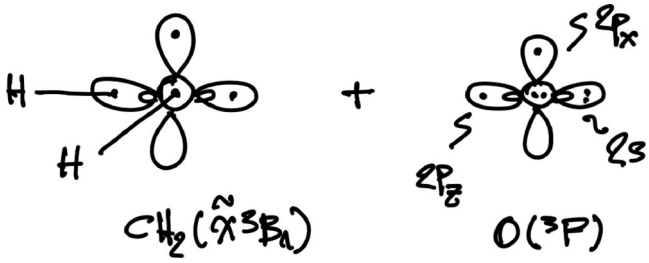


**Scheme 1.** vbL diagram depicting the $CH_2$ ($\tilde{X}^3B_1$) + O ($^3$P) interaction.

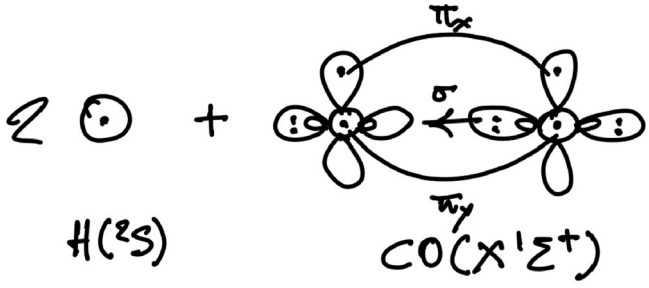


**Scheme 2.** vbL diagram depicting the 2H ($^2$S) + CO ($X^1\Sigma^+$) interaction.

In the first case (see Scheme 1) the two fragments, $CH_2$ and O are ready to bind together through a sigma and pi bonds. In the second case (see Scheme 2) all CO electrons are singlet coupled into pairs thus giving no opportunity to the two incoming (in a $C_{2v}$ way) H atoms to bind. Two unpaired electrons that are 'ready' for bond formation are present in the $a^3\Pi$ state but a high energetic price has to be paid ($T_e$ (exp) = 139.2 kcal/mol, [39]). Despite the energy amount to reach this highly excited state there is no other way to form two CH bonds and this is visible in Figure 1 that portrays the energy profiles of the 2H ($^2$S) + CO ($X^1\Sigma^+/a^3\Pi$) interaction at the MRCI level of theory when the two H atoms approach the CO moiety along a $C_{2v}$ reaction path by maintaining the CO distance at the equilibrium geometry of $H_2CO$ ($\tilde{X}^1A_1$). It is obvious from the curves along this formation path that there is an interaction between the energy profiles stepping from the 2H ($^2$S) + CO ($X^1\Sigma^+/a^3\Pi$) asymptotic channels with a peak at around 4 bohr and this is substantiated by the evolution of the NACMEs along the evolution path as shown in Figure 2 where we can see the 'change' of electronic character between the states arising from 2H ($^2$S) + CO ($X^1\Sigma^+/a^3\Pi$). This behaviour is 'logical' if one considers the details of the electronic structure of CO at both its ground ($X^1\Sigma^+$) and first excited ($a^3\Pi$) states. Their CASSCF equilibrium characteristics are given below (counting only valence electrons)

$$|X^1\Sigma^+(^1A_1)\rangle \cong |1\sigma^2 2\sigma^2 3\sigma^2[0.97 \times 1\pi_x^2 1\pi_y^2 - 0.10 \times (1\pi_x^2 2\pi_y^2 + 2\pi_x^2 1\pi_y^2)]\rangle - 0.12|1\sigma^2 2\sigma^2 3\sigma^2 1\pi_x^1 2\bar{\pi}_x^1 1\pi_y^1 2\bar{\pi}_y^1\rangle$$

$$C(2s^{1.85}2p_z^{0.91}2p_x^{0.53}2p_y^{0.53}) \quad \text{and}$$
$$O(2s^{1.76}2p_z^{1.43}2p_x^{1.40}2p_y^{1.40})$$

$$1\sigma \cong 2s(O),\ 2\sigma \cong -0.34 \times 2s(C) - 0.67 \times 2p_z(C) + 0.80 \times 2p_z(O),$$
$$3\sigma \cong 0.84 \times 2s(C) - 0.43 \times 2p_z(C) - 0.32 \times 2s(O)$$

and

$$|a^3\Pi(^3B_1)\rangle \cong |1\sigma^2 2\sigma^2 3\sigma^1 1\pi_x^2 2\pi_x^1 1\pi_y^2\rangle - 0.15|1\sigma^2 2\sigma^2 3\sigma^1 1\pi_x^2 2\pi_x^1 1\bar{\pi}_y^1 2\pi_y^1\rangle$$

$C(2s^{1.17}2p_z^{0.62}2p_x^{1.20}2p_y^{0.69})$ and

$O(2s^{1.82}2p_z^{1.34}2p_x^{1.73}2p_y^{1.28})$

$1\sigma \cong 2s(O)$,

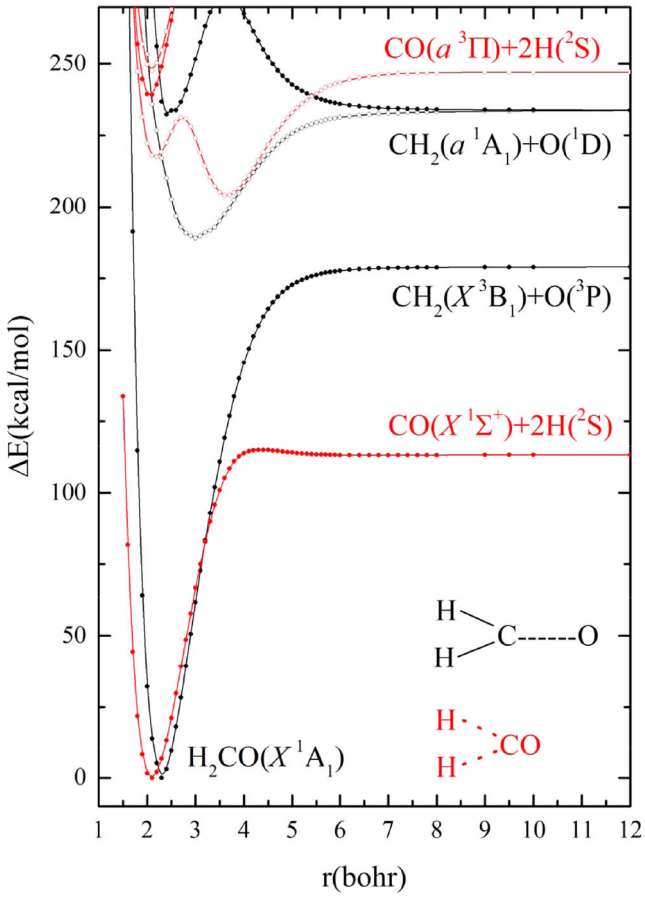


**Figure 1.** Potential energy profiles of the ground $\tilde{X}^1A_1$ $H_2CO$ state along the $H_2C + O$ (black colour; the reaction coordinate r measures the distance between $H_2C$ and O along a $C_{2v}$ path) and $2H + CO$ (red colour; the reaction coordinate r measures the distance between 2H and CO along a $C_{2v}$ path) $C_{2v}$ dissociation paths at the MRCI/cc–pVQZ level of theory. The geometry of the molecular fragments ($CH_2$ and CO) is at the equilibrium structure of $H_2CO$ ($\tilde{X}^1A_1$) (see Table 1).

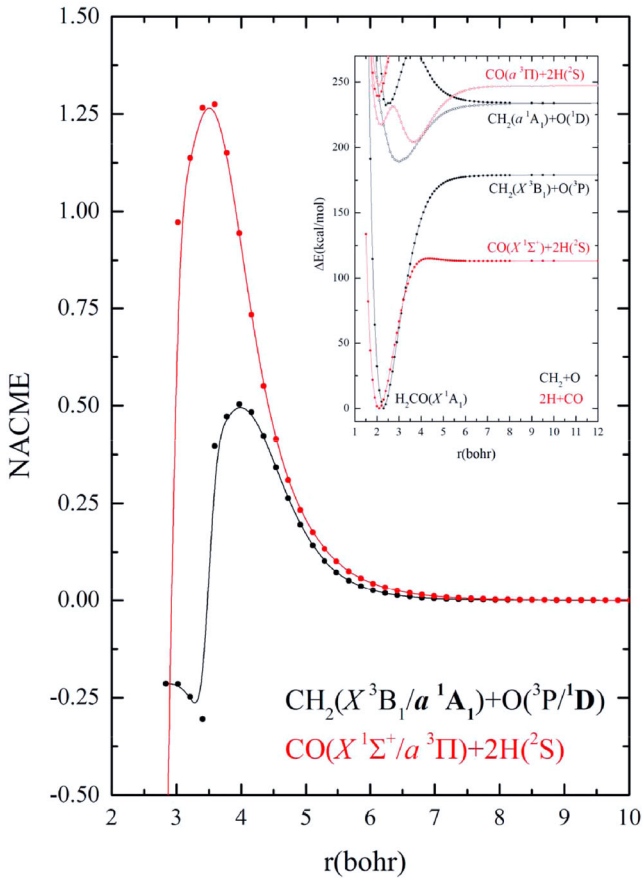


**Figure 2.** NACMEs between $H_2CO$ states of $^1A_1$ symmetry along the $H_2C + O$ (black colour) and $2H + CO$ (red colour) $C_{2v}$ dissociation paths at the CASSCF/cc–pVQZ level of theory. The reaction coordinate r is as defined in Figure 1.

$$2\sigma \cong -0.69 \times 2s(\mathrm{C}) - 0.35 \times 2p_z(\mathrm{C}) + 0.73 \times 2p_z(\mathrm{O}),$$

$$3\sigma \cong 0.70 \times 2s(\mathrm{C}) - 0.68 \times 2p_z(\mathrm{C}) + 0.35 \times 2p_z(\mathrm{O})$$

All the above are clearly captured by the vbL icons of Scheme 3.

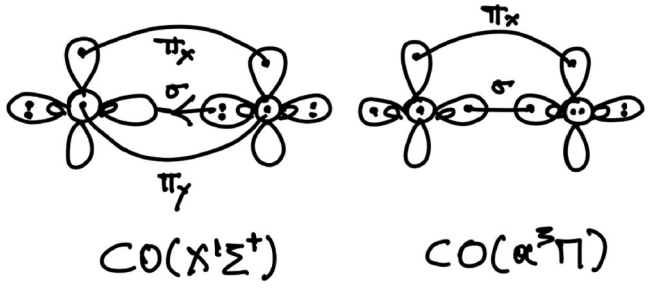


**Scheme 3.** vbL diagrams depicting the $X^1\Sigma^+$ and $a^3\Pi$ CO states.

As we can see the $a^3\Pi$ CO state is 'ready' to form two CH bonds with its two triplet coupled carbon–based electrons. It is also illuminating to ponder on the structural characteristics of $CH_2$ ($\tilde{X}^3B_1$ and $\tilde{a}^1A_1$), CO ($X^1\Sigma^+$ and $a^3\Pi$), and $H_2CO$ ($\tilde{X}^1A_1$) (see Table 1): HCH (angle) = 133.47° / 102.05° ($CH_2$; $\tilde{X}^3B_1$ / $\tilde{a}^1A_1$), 116.20° ($H_2CO$; $\tilde{X}^1A_1$) and CO (distance) = 1.132 Å / 1.209 Å (CO; $X^1\Sigma^+/a^3\Pi$), 1.206 Å ($H_2CO$; $\tilde{X}^1A_1$). Although the CO distance in $H_2CO$ ($\tilde{X}^1A_1$) is identical to the distance of free CO ($a^3\Pi$) its HCH angle is not the same as the one in $CH_2$ ($\tilde{X}^3B_1$) but it is essentially equal to the average (118.5°) of both $\tilde{X}^3B_1$ and $\tilde{a}^1A_1$. This may seem surprising at first sight but it can be rationalised when we look at the energy profiles along the $H_2C + O$ $C_{2v}$ interaction path (see Figure 1); the O atom approaches $CH_2$ along its $C_{2v}$ axis with the $CH_2$ geometry at the equilibrium values of $H_2CO$ ($\tilde{X}^1A_1$). Although formaldehyde's ground state dissociates adiabatically to ground state fragments, $CH_2$ ($\tilde{X}^3B_1$) + O ($^3P$), the potential curve arising from $CH_2$ ($\tilde{a}^1A_1$) + O ($^1D$) makes a sensible participation (the max value of the corresponding NACMEs is less than half

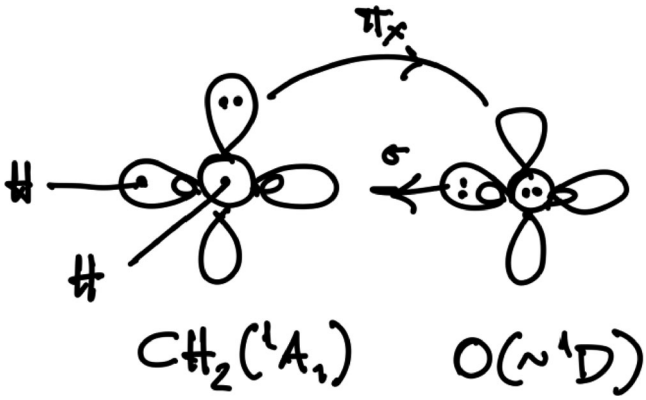


**Scheme 4.** vbL diagram depicting the $CH_2$ ($^1A_1$) + O ($\sim$ $^1D$) interaction.

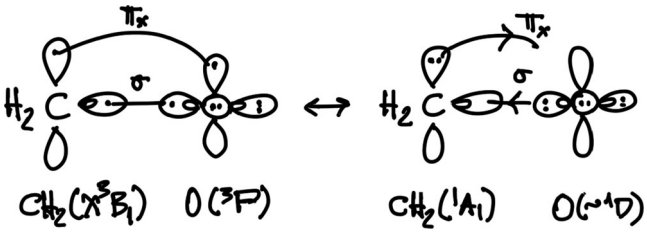


**Scheme 5.** vbL diagram depicting $H_2CO(\tilde{X}^1A_1)$ as a resonance of two structures.

the peak value along the CO + 2H $C_{2v}$ reaction path) as evidenced from the evolution of the NACMEs in Figure 2. This kind of $\tilde{X}^3B_1/\tilde{a}^1A_1$ interaction compensates for the high excitation energy of the CO $X^1\Sigma^+ \rightarrow a^3\Pi$ *in situ* transition. $H_2CO$ ($\tilde{X}^1A_1$)'s main CASSCF equilibrium configuration are

$$|\tilde{X}^1A_1\rangle \cong |1a_1^2 2a_1^2 3a_1^2 (0.96 \times 1b_1^2 - 0.15 \times 2b_1^2) 1b_2^2 2b_2^2\rangle$$

with $3a_1 \cong -0.67 \times 2p_z(C) + 0.75 \times 2p_z(O)$ and $2s^{1.15}(C)$. The second way of interaction is depicted in the vbL diagram of Scheme 4.

So, ground state $H_2CO$ is a hybrid of two bonding patterns accommodating this way for both its electronic and structural characteristics, see *e.g.* Scheme 5.

Now, let us move to the fluoro–substituted formaldehyde, $F_2CO$, carbonyl fluoride that will serve as a bridge between $H_2CO$ and $(HO)_2CO = H_2CO_3$ (isoelectronic to $F_2CO$). $CF_2$'s ground state is of $^1A_1$ symmetry while its first excited state is of $^3B_1$ symmetry quite the opposite from the $CH_2$ case (see Table 1). As already discussed in the $H_2CO$ case, there are two formation/dissociation channels, the $F_2C + O \rightarrow F_2CO$ and $F_2CO \rightarrow 2F + CO$ (see Figure 3); the O atom approaches $F_2C$ along its $C_{2v}$ axis while maintaining the $F_2C$ species in the equilibrium geometry of $F_2CO$ ($\tilde{X}^1A_1$), while the 2F atoms approach CO along a $C_{2v}$ reaction path by maintaining the CO

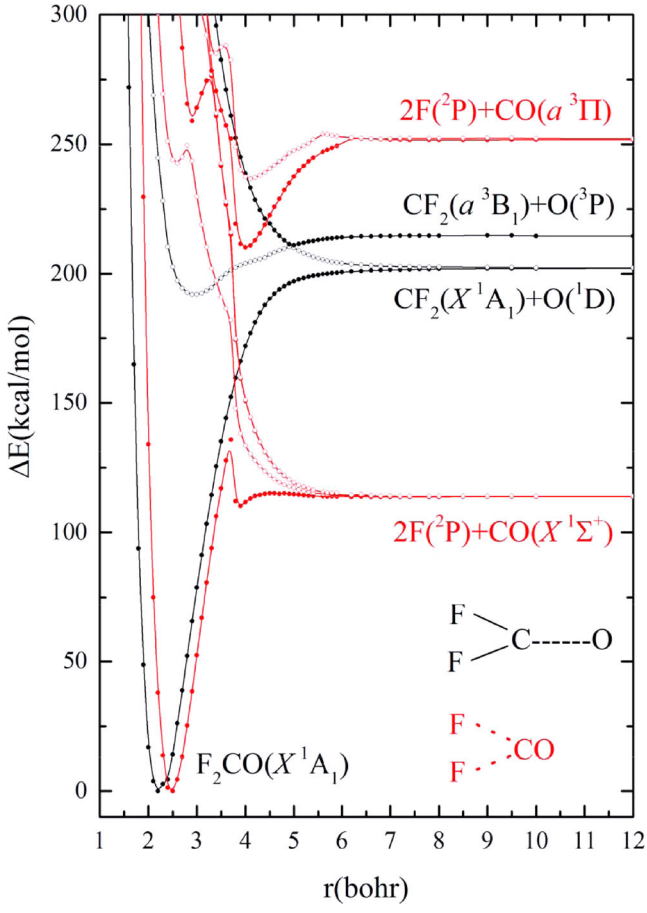


**Figure 3.** Potential energy profiles of the ground $\tilde{X}^1A_1$ $F_2CO$ state along the $F_2C + O$ (black colour; the reaction coordinate r measures the distance between $F_2C$ and O along a $C_{2v}$ path) and 2F + CO (red colour; the reaction coordinate r measures the distance between 2F and CO along a $C_{2v}$ path) $C_{2v}$ dissociation paths at the MRCI/cc–pVQZ level of theory. The geometry of the molecular fragments ($CF_2$ and CO) is at the equilibrium structure of $F_2CO$ ($\tilde{X}^1A_1$) (see Table 1).

distance at the equilibrium geometry of $F_2CO$ ($\tilde{X}^1A_1$). In the latter ($F_2CO \rightarrow 2F + CO$) case the energy profiles are quite revealing. It is the energy profile arising from the 2F ($^2P$) + CO ($a^3\Pi$) asymptotic channel that is responsible for the $F_2CO$ ($\tilde{X}^1A_1$) minimum through an avoided crossing peaked at around 4 bohr and this is in harmony with the interaction of the profiles converging to $CF_2$ ($\tilde{X}^1A_1$) + O ($^1D$) and $CF_2$ ($\tilde{a}^3B_1$) + O ($^3P$). The structural characteristics of both the asymptotic fragments and the final species follow (see Table 1): FCF (angle) = 104.98° / 119.28° ($CF_2$; $\tilde{X}^1A_1/\tilde{a}^3B_1$), 107.82° ($F_2CO$; $\tilde{X}^1A_1$) and CO (distance) = 1.132 Å / 1.209 Å (CO; $X^1\Sigma^+/a^3\Pi$), 1.174 Å ($F_2CO$; $\tilde{X}^1A_1$). The Mulliken atomic population of the C atom in $F_2CO$ ($\tilde{X}^1A_1$) is just $2s^{0.85}$ while in free $CF_2$ is $2s^{1.70}(\tilde{X}^1A_1)$ and $2s^{1.11}(\tilde{a}^3B_1)$ thus alluding to a heavy participation of $CF_2$ ($\tilde{a}^3B_1$) in the formation of $F_2CO$ while its equilibrium CASSCF

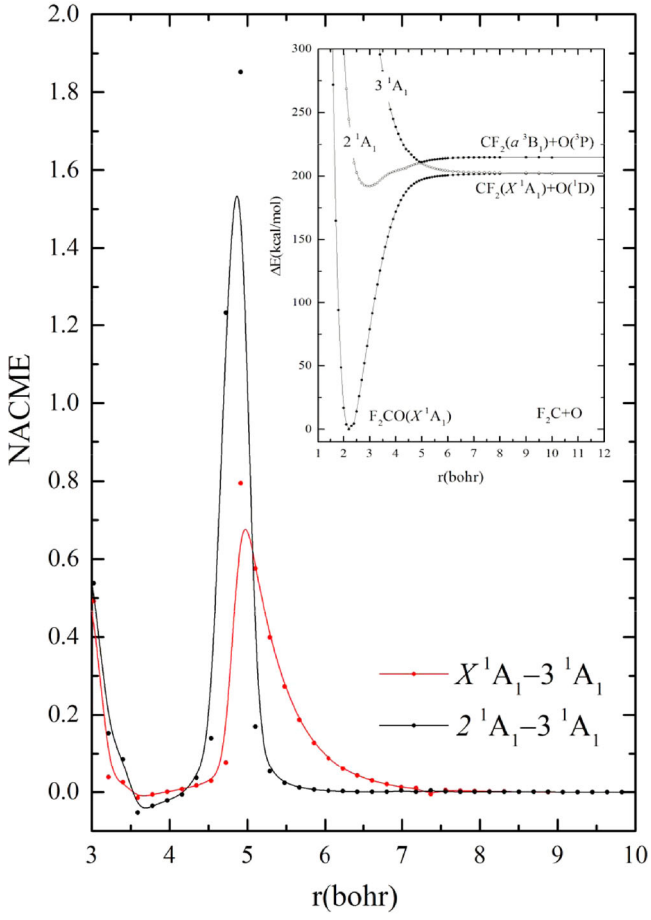


**Figure 4.** NACMEs between $F_2CO$ states of $^1A_1$ symmetry along the $F_2C + O$ $C_{2v}$ dissociation path at the CASSCF/cc–pVQZ level of theory. The reaction coordinate r is as defined in Figure 3.

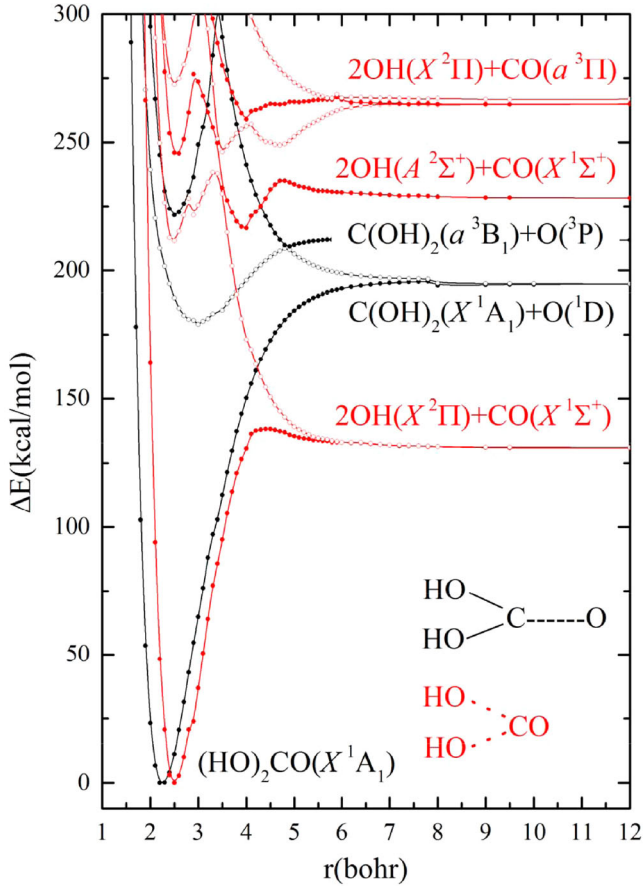


**Figure 5.** Potential energy profiles of the ground $\tilde{X}^1A_1$ $(HO)_2CO$ state along the $(HO)_2C + O$ (black colour; the reaction coordinate r measures the distance between $(HO)_2C$ and O along a $C_{2v}$ path) and $2OH + CO$ (red colour; the reaction coordinate r measures the distance between 2OH and CO along a $C_{2v}$ path) $C_{2v}$ dissociation paths at the MRCI/cc–pVQZ level of theory. The geometry of the molecular fragments ($C(OH)_2$ and CO) is at the equilibrium structure of $(OH)_2CO$ ($\tilde{X}^1A_1$) (see Table 1).

wavefunction is *mutatis mutandis* analogous to that of $H_2CO$;$|\tilde{X}^1A_1\rangle \cong |1a_1^2 2a_1^2 3a_1^2 4a_1^2 5a_1^2 1b_1^2 (0.97 \times 2b_1^2 - 0.11 \times 3b_1^2) 1b_2^2 2b_2^2 3b_2^2 4b_2^2 1a_2^2\rangle$. The involvement of $CF_2$ ($\tilde{a}^3B_1$) is also corroborated by the evolution of the NACMEs along the relevant formation path as shown in Figure 4.

Having studied $F_2CO$ we are now in position to tackle carbonic acid, $(HO)_2CO = H_2CO_3$, isoelectronic to carbonyl fluoride, $F_2CO$. As we have done before we shall study both formation routes, *i.e.* $2\ OH + CO \rightarrow (HO)_2CO \leftarrow (HO)_2C + O$. The energy profiles are displayed in Figure 5 and are in striking similarity with those of the $F_2CO$ species shown in Figure 3. This is to be expected not only because of the 'isoelectronicity' of both systems but also because of the fact that both $(HO)_2C$ and $F_2C$ fragments have the same energetic blueprint (see Table 1). Carbonic acid's equilibrium minimum is due to the $C(OH)_2$ $(\tilde{a}^3B_1) + O$ ($^3$P) and/or $2OH(X^2\Pi) + CO$ $(a^3\Pi)$ interaction in the latter case through the intermediate of the $2OH(X^2\Sigma^+) + CO$ $(X^1\Sigma^+)$ profile (see Figure 5). The equilibrium characteristics of both the asymptotic and the final species are interesting to compare: (HO)C(OH) (angle) = 104.77° / 116.04° ($C(OH)_2$; $\tilde{X}^1A_1$/ $\tilde{a}^3B_1$), 108.63° ($(HO)_2CO$; $\tilde{X}^1A_1$) and CO (distance) = 1.132 Å / 1.209 Å (CO; $X^1\Sigma^+$/ $a^3\Pi$), 1.203 Å ($(HO)_2CO$; $\tilde{X}^1A_1$), practically identical to the ones found in $F_2CO$ (*see above*). The Mulliken atomic population of the C atom in $(HO)_2CO$ ($\tilde{X}^1A_1$) is only $2s^{0.88}$ while in $C(OH)_2$ is $2s^{1.77}(\tilde{X}^1A_1)$ and $2s^{1.17}(\tilde{a}^3B_1)$ suggesting that way the participation of $C(OH)_2$ $(\tilde{a}^3B_1)$ and/or CO $(a^3\Pi)$ states in carbonic acid's equilibrium geometry while its equilibrium CASSCF wavefunction is similar to those of both $H_2CO$ and $F_2CO$;

$$|\tilde{X}^1A_1\rangle \cong 0.97|1a_1^2 2a_1^2 3a_1^2 4a_1^2 5a_1^2 1b_1^2 2b_1^2 1b_2^2 2b_2^2 \times 3b_2^2 4b_2^2 1a_2^2\rangle$$

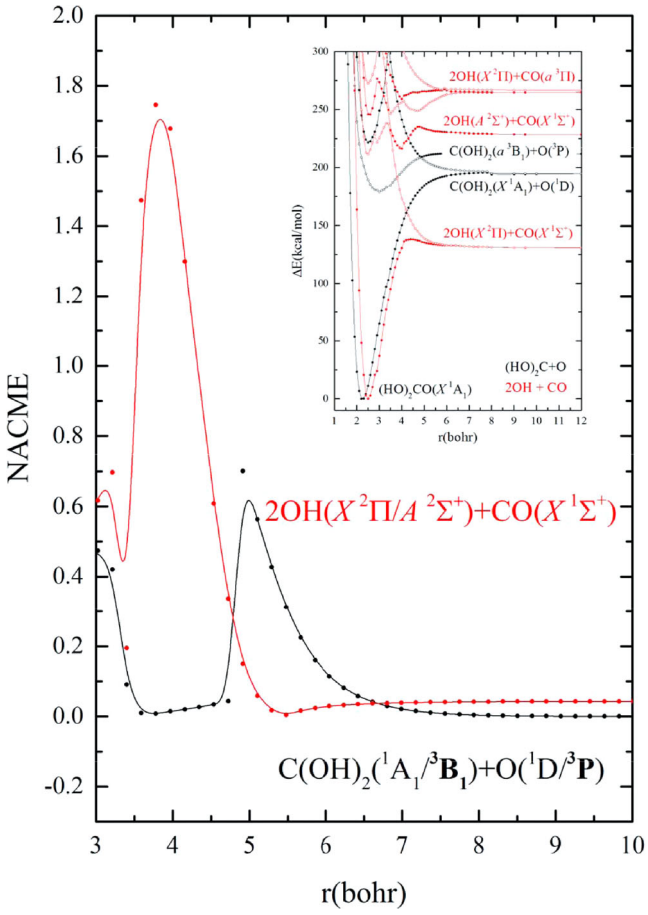


**Figure 6.** NACMEs between $(HO)_2CO$ states of $^1A_1$ symmetry along the $(HO)_2C + O$ (black colour) and $2OH + CO$ (red colour) $C_{2v}$ dissociation paths at the CASSCF/cc–pVQZ level of theory. The reaction coordinate r is as defined in Figure 6.

$$+ 0.12|1a_1^2 2a_1^2 3a_1^2 4a_1^2 5a_1^2 1b_1^2 2b_1^1 3\bar{b}_1^1 1b_2^2 2b_2^2 \times 3b_2^2 4b_2^2 1a_2^2\rangle$$

This is also supported by the evolution of the NACMEs along both formation routes shown in Figure 6 which displays the character blending of the wavefunctions associated with the $C(OH)_2$ $(\tilde{X}^1A_1/\tilde{a}^3B_1) + O$ $(^1D/^3P)$ and $2OH(X^2\Pi/X^2\Sigma^+) + CO$ $(X^1\Sigma^+)$ energy profiles, featuring a peak at around 5 and 4 bohr, respectively.

## 4. Conclusions

Carbon is a tetravalent atom and as such it can use all four of its valence electrons in the formation of molecular species. This is true for all of the species presently studied, *i.e.* $H_2CO$, $F_2CO$ and $(HO)_2CO$ $(= H_2CO_3)$ and it was shown rather eloquently by both the energy profiles along the formation paths $X_2C + O$ and/or $2X + CO$ (X = H, F, and OH) and the evolution of the non adiabatic coupling matrix elements along the same formation channels. Through a comparative study of the fragmentary species $CX_2$ and CO and the final species $X_2CO$ we are able to appreciate the importance of the excited states' participation in the formation of the $X_2CO$ ground state through the sequence $C(^5S) \rightarrow CX_2$ $(^3B_1)$ or CO $(a^3\Pi)$ $\rightarrow X_2CO$ $(\tilde{X}^1A_1)$.

## Disclosure statement

No potential conflict of interest was reported by the author(s).

## ORCID

*Apostolos Kalemos* http://orcid.org/0000-0002-1022-0029

## References

[1] S. Thoms, J. Theor. Biology. 215, 399–404 (2002). doi:10.1006/jtbi.2002.2528.
[2] T.H. Maren, Physiol. Rev. 47, 595–781 (1967). doi:10.1152/physrev.1967.47.4.595.
[3] J.C. Orr, V.J. Fabry, O. Aumont, L. Bopp, S.C. Doney, R.A. Feely, A. Gnanadesikan, N. Gruber, F. Joos, *et al.*, Nature. 437, 681–686 (2005). doi:10.1038/nature04095.
[4] H. Mohr and P. Schofper, *Plant Physiology* (Springer–Verlag, Berlin–Heidelberg, 1995).
[5] J.K. Terlouw, C.B. Lebrilla and H. Schwarz, Angew. Chem. Int. Ed. Engl. 26, 354–355 (1987). doi:10.1002/anie.198703541.
[6] T. Mori, K. Suma, Y. Sumiyoshi, and Y. Endo, J. Chem. Phys. 130, 204308 (1–7) (2009). doi:10.1063/1.3141405.
[7] T. Mori, K. Suma, Y. Sumiyoshi, and Y. Endo, J. Chem. Phys. 134, 044319 (1– 6) (2011). doi:10.1063/1.3532084.
[8] J. Bernard, M. Siedl, I. Kohl, K.R. Liedl, E. Mayer, O. Galvez, H. Grothe and T. Loerting, Angew. Chem. Int. Ed. Engl. 50, 1939–1943 (2011). doi:10.1002/anie.201004729.
[9] J. Bernard, R.G. Huber, K.R. Liedl, H. Grothe and T. Loerting, J. Am. Chem. Soc. 135, 7732–7737 (2013). doi:10.1021/ja4020925.
[10] H.P. Reisenauer, J.P. Wagner and P.R. Schreiner, Angew. Chem. Int. Ed. Engl. 53, 11766–11771 (2014). doi:10.1002/anie.201406969.
[11] S. Ghoshal and M.K. Hazra, RSV Adv. 5, 17623–17635 (2015). doi:10.1039/C4RA13233E.
[12] B. Jönsson, G. Karlström, H. Wennerström and B. Roos, Chem. Phys. Lett. 41, 317–320 (1976). doi:10.1016/0009-2614(76)80819-6.
[13] K.B. Wiberg and K.E. Laidig, J. Am. Chem. Soc. 109, 5935–5943 (1987). doi:10.1021/ja00254a006.
[14] R. Janoschek and I.G. Csizmadia, J. Mol. Struct. 300, 637–645 (1993). doi:10.1016/0022-2860(93)87052-B.
[15] C.A. Wight and A.I. Boldyrev, J. Phys. Chem. 99, 12125–12130 (1995). doi:10.1021/j100032a012.
[16] C.S. Tautermann, A.F. Voegele and K.R. Liedl, J. Chem. Phys. 120, 631–637 (2004). doi:10.1063/1.1630565.
[17] H-G Yu, J.T. Muckerman and J.S. Francisco, J. Phys. Chem. A. 109, 5230–5236 (2005). doi:10.1021/jp051458w.
[18] Y-J Wu, C.Y. Robert Wu and M-C Liang., Icarus. 214, 228–235 (2011). doi:10.1016/j.icarus.2011.05.009.

[19] S.E. Huber, S. Dalnodar, W. Kausch, S. Kineswenger, and M. Probst, AIP Adv. 2, 032180 (1–15) (2012). doi:10.1063/1.4755786.
[20] S.A. de Marothy, Int. J. Quantum Chem. 113, 2306–2311 (2013). doi:10.1002/qua.24452.
[21] J. Philip Wagner, H. Peter Reisenauer, V. Hirvonen, C.-H. Wu, J.L. Tyberg, W.D. Allen and P.R. Schreiner, Chem. Comm. 52, 7858–7861 (2016). doi:10.1039/C6CC01756H.
[22] D. Pines, J. Ditkovich, T. Mukra, Y. Miller, P.M. Kiefer, S. Daschakraborty, J.T. Hynes and E. Pines, J. Phys. Chem. B. 120, 2440–2451 (2016). doi:10.1021/acs.jpcb.5b12428.
[23] L. Sagiv, B. Hirschberg and R.B. Gerber, Chem. Phys. 514, 44–54 (2018). doi:10.1016/j.chemphys.2017.12.015.
[24] S. Mallick and P. Kumar, Phys. Chem. Chem. Phys. 21, 20849–20856 (2019). doi:10.1039/C9CP04587B.
[25] S. Shaik, D. Danovich and P.C. Hiberty, Comp. Theor. Chem. 1116, 242–249 (2017). doi:10.1016/j.comptc.2017.01.017.
[26] L.T. Xu and T.H. Dunning, Jr., J. Phys. Chem. A 124, 204–214 (2020). doi:10.1021/acs.jpca.9b11054.
[27] S. Böhm, D. Antipova and J. Kuthan, Int. J. Quantum Chem. 62, 315–322 (1997). doi:10.1002/(SICI)1097-461X(1997)62:3 < 315::AID-QUA10 > 3.0.CO;2-8.
[28] G. Saleh and A.R. Oganov, Sci. Rep. 6, 32486 (1–9) (2016). doi:10.1038/srep32486.
[29] H. Bassett, Justus. Liebigs. Ann. Chem. 132, 54–61 (1864). doi:10.1002/jlac.18641320106.
[30] M. Igarashi, T. Matsumoto, F. Yagihashi, H. Yamashita, T. Ohhara, T. Hanashima, A. Nakao, T. Moyoshi, K. Sato, and S. Shimada, Nat. Commun. 8, 140 (1–8) (2017). doi:10.1038/s41467-017-00168-5.
[31] L.M. Jurkić, I. Cepanec, S.K. Pavelić, and K. Pavelić, Nutrition Metabolism 10, 2 (1–12) (2013). doi:10.1186/1743-7075-10-2.
[32] T.H. Dunning Jr., J. Chem. Phys. 90, 1007–1023 (1989). doi:10.1063/1.456153.
[33] MOLPRO is a package of *ab initio* programs written by H.—J. Werner, P. J. Knowles, G. Knizia, F. R. Manby, M. Schütz, P. Celani, W. Györffy, D. Kats, T. Korona, R. Lindh, A. Mitrushenkov, G. Rauhut, K. R. Shamasundar, T. B. Adler, R. D. Amos, A. Bernhardsson, A. Berning, D. L. Cooper, M. J. O. Deegan, A. J. Dobbyn, F. Eckert, E. Goll, C. Hampel, A. Hesselmann, G. Hetzer, T. Hrenar, G. Jansen, C. Köppl, Y. Liu, A. W. Lloyd, R. A. Mata, A. J. May, S. J. McNicholas, W. Meyer, M. E. Mura, A. Nicklaß, D. P. O'Neill, P. Palmieri, D. Peng, K. Pflüger, R. Pitzer, M. Reiher, T. Shiozaki, H. Stoll, A. J. Stone, R. Tarroni, T. Thorsteinsson and M. Wang.*MOLPRO*, *version 2012.1*, *a package of ab initio programs*; University College Cardiff Consultants Limited: Cardiff, U.K., 2008.
[34] P. Jensen and P.R. Bunker, J. Chem. Phys. 89, 1327–1332 (1988). doi:10.1063/1.455184.
[35] A. Kalemos, T.H. Dunning, Jr., A. Mavridis and J.F. Harrison, Can. J. Chem. 82, 684–693 (2004). doi:10.1139/v04-045.
[36] L.T. Xu, J.V.K. Thompson and T.H. Dunning, Jr., J. Phys. Chem. A. 123, 2401–2419 (2019). doi:10.1021/acs.jpca.9b00376.
[37] A. Kramida, Yu. Ralchenko, J. Reader, and NIST ASD Team (2020). *NIST Atomic Spectra Database* (ver. 5.8), [Online]. Available: https://physics.nist.gov/asd. National Institute of Standards and Technology, Gaithersburg, MD. doi:10.18434/T4W30F.
[38] F. Fantuzzi, D.W.O. de Sousa and M.A.C. Nascimento, Chem. Select. 2, 604–619 (2017).
[39] "Constants of Diatomic Molecules" by K.P. Huber and G. Herzberg (data prepared by J.W. Gallagher and R.D. Johnson, III) in NIST Chemistry WebBook, NIST Standard Reference Database Number 69, Eds. P.J. Linstrom and W.G. Mallard, National Institute of Standards and Technology, Gaithersburg MD, 20899, doi:10.18434/T4D303.